Progress in Flight Physics **7** (2015) 525-548
DOI: 10.1051/eucass/201507525

ON MODELING OF LAMINAR–TURBULENT TRANSITION IN SUPERSONIC FLOWS WITH ENGINEERING CORRELATIONS AND REYNOLDS-AVERAGED NAVIER–STOKES EQUATIONS

R. V. Kovalev, V. V. Kudryavtsev, and D. A. Churakov

Central Research Institute of Machine Building, Russian Space Agency (TsNIIMash)
4 Pionerskaya Str., Korolev, Moscow Region 141070, Russia

This paper deals with different engineering correlations for prediction of transitional hypersonic flows both for transition onset prediction and transition zone description. In spite of recent progress in simulation of stability equations and direct methods, these approaches remain main tool in everyday design practice. Very close approach is using correlations incorporated in the Reynolds-averaged Navier–Stokes (RANS) equations, e. g., γ–Re_θ transition model. But this model has some limitations when applied to supersonic flows and some approaches for subduing these limitations are considered. Also, the effect of local heating/cooling on laminar–turbulent transition (LTT) on sharp cone is analyzed on the basis of both algebraic correlations and RANS models.

1 INTRODUCTION

Prediction of LTT onset in supersonic and hypersonic flows is one of the most important problems still unsolved in applied aeromechanics. In spite of doubtless progress in transition modeling on the basis of physical approaches such as linear stability theory and direct numerical simulation with unsteady Navier–Stokes equations, empirical approaches based on simple correlations have to be used in engineering practice. Multifactor nature of LTT and possibility of different transition scenarios [1] give rise to significant uncertainties in such

correlation formulas. Because of elevated magnitude of turbulent heat transfer (compared to laminar flows), these uncertainties in LTT prediction lead to "conservative" estimations of transition to turbulence for space vehicles flight trajectories that, in turn, lead to extra weights of vehicle thermal protection system (TPS).

Multifactor nature of LTT (dependence of LTT on large amount of aerophysical phenomena — flow compressibility, inflow disturbance level, surface roughness, nose bluntness and angle of attack, influence of surface blowing or suction, etc.) does not allow simultaneous accounting for effect of all those interacting factors on the boundary layer transition.

Understanding of general laws of LTT development and possibility of transition control require separate analysis of these effects to be made. One possibility of such transition control in supersonic flow is heating/cooling of a vehicle surface. It is long known that surface temperature may have dual influence on the LTT onset in supersonic flow conditions. On the one hand, surface cooling may lead to damping of first unstable disturbance mode and move LTT downstream, but on the other hand, it may lead to the growth of second mode and acceleration of LTT.

Local (stripwise) surface heating/cooling may also result in either increase or decrease of boundary layer receptivity to the disturbances [2]. This effect (influence of local heating/cooling on LTT control) was intensively studied within a TransHyBeriAN project of European Union's Seventh Framework Programme (EU FP7) [3]. A simple generic form — 7 degree sharp cone with narrow heated/cooled ring strip near the nose in $M \approx 6$ supersonic flow — was selected for experiments and numerical treatments.

This paper deals with two possible means for theoretical prediction of LTT for this test conditions. First tool is empirical algebraic correlations usual in the spacecraft design practice. Different empirical approximations for LTT onset prediction were analyzed and compared in order to realize their possibility of accounting for the effect of local heating/cooling on LTT. Also, different empirical approaches for simulation of transition zone extension were considered.

Another way for theoretical prediction of the LTT and estimation of local thermal control closely related to using correlations is RANS equations with additional equations for simulation of transition. The γ–Re_θ model [4] together with k–ω shear stress transport (SST) turbulent viscosity differential model [5] is used here for these purposes. As a matter of fact, this approach is a method of incorporation of correlation relationships into modern computational fluid dynamics (CFD) codes based on numerical integration of RANS equations. Originally developed for modeling incompressible or weakly-compressible flows, this method encounters some difficulties when applied to simulation of flows at higher Mach numbers. This paper also addresses the reasons for origination of these difficulties and some ways for their elimination are proposed.

2 ENGINEERING ALGEBRAIC CORRELATIONS FOR TRANSITION PREDICTION

Most of engineering algebraic transition correlations can be considered as consisting of two different parts. First, it is some correlation for prediction of transition onset and second, some correlation for prediction transition zone spread and variation of turbulent intermittency within it. In most cases, these two parts can be arbitrary mixed and one can consider them separately.

There are many different correlations for the transition onset prediction in the literature [6]. They were developed for certain practical engineering demands and in the situation of lack of reliable instruments for prediction of LTT onset with more physical ground (that is, using actual consideration of the flow instability and disturbance growth), these models are still the main predictive tool in engineering practice. All these models are compulsory empirical and based on experimental data obtained either in ground-based facilities or in free-flight conditions. Empirical character of these criteria often leads to their restricted applicability. As LTT is very complex physical phenomenon, ruled by diversity of different factors, followed to different scenarios and affected by very small disturbances, etc., most of empirical correlations can be applied only to rather limited classes of bodies and restricted ranges of flow conditions.

These empirical criteria are usually local ones, that is, they include only local integral boundary-layer and boundary-layer edge-flow properties. This means that all the phenomena connected to propagation and development of small, medium, and large scale disturbances cannot be taken into account explicitly. At best, some flow prehistory can be implicitly accounted for via some integral boundary-layer quantity. Test data obtained in usual ground-based facilities (if these are not "quite" tunnels, those are dramatically rare) are possibly contaminated with the tunnel noise effects. It leads to separation of the correlations onto "on-ground" and "free-flight" branches that also cannot add clarity to the LTT phenomenon. Moreover, these correlations are of "two-dimensional" nature and there is no straightforward generalization of them for real three-dimensional (3D) situations, though they were utilized in practice for transition predictions for complex geometries (e. g., Space Shuttle) without sufficient physical ground.

Due to their empirical character, all these correlations include one or more "tuning" constants, which values can vary within wide range of magnitude to cover available experimental data. This extension of the applicability range also brings about widening of uncertainty in the transition onset position if this correlation is applied to a certain flight vehicle. As a result, in terms of flight altitude, this uncertainty in LTT onset can reach several (if not tens) kilometers.

As devised for practical needs, such correlations use "heat flux growth start position" for specification of LTT onset even though actual level of disturbances

in the boundary layer at that position may be very high and all linear growth part of transition region can lie far upstream of that point. Actually, in such consideration, the transition region is a part of flow with very rapid nonlinear growth of disturbances with remarkable spotting of developed turbulence.

General flow parameters involved in such correlations are:

- local boundary layer outer edge parameters (subscript "e") — velocity, Mach number, pressure, viscosity, density, etc. — U_e, M_e, P_e, T_e, μ_e, ρ_e, etc.;
- local wall parameters (subscript "w") — T_w, μ_w, ρ_w, etc.;
- some integral thickness of the boundary layer; in most cases, it is momentum thickness

$$\theta = \int_0^\delta \frac{u}{U_e}\left(1 - \frac{\rho u}{\rho_e U_e}\right) dy$$

  as the thickness which value affected by compressibility to the less extent compared to other integral thicknesses;
- specific parameters initiating or affecting transition process: effective wall roughness height — k_w, free stream turbulence level — Tu,

$$\mathrm{Tu} = \sqrt{\frac{u'^2 + v'^2 + w'^2}{3U_\infty^2}},$$

  etc.

Dimensional parameters can be grouped in nondimensional combinations forming new set of independent variables and leading to transition correlation in criterial form, for which the properly normalized transition onset position depends only on nondimensional parameters. There is a single exception from this rule, when "unit Reynolds number" $\mathrm{Re}_1 = \rho_e U_e/\mu_e$ with dimension of inverse length is used as a parameter in expressions for transition onset specification. Actually, unit Reynolds number is used in correlations as it would be nondimensional. Thus, there is no physical sense in its using in nondimensional correlations. On the other hand, there are sufficiently many experimental evidences where this unit Reynolds number influences the transition onset in a drastic way. This paradoxical situation can be explained only by the assumption that in all these experiments, there was some "hidden" additional parameter with dimension of length and its magnitude is about of the same order for close groups of tests. This may be some average surface roughness height for usual test models or some characteristic scale of inflow disturbances for the on-ground facilities of the same type or something else of this kind. Anyway,

this scale have to be approximately the same for different usual ground-based facilities if no special care have not been taken on preventing of impact of this scale, such as using quite wind tunnels, perfectly smooth model surfaces, and so on.

A typical example of smooth body criteria is a correlation [7] for critical transitional momentum thickness Reynolds number

$$\mathrm{Re}_{\theta,\mathrm{tr}} = A \exp\left(\beta \mathrm{M}_e\right) ; \quad \mathrm{Re}_\theta = \frac{\rho_e U_e \theta}{\mu_e} . \tag{1}$$

Two empirical constants are used here with variation accepted to be in the range $100 \le A \le 300$ and $0.1 \le \beta \le 0.2$. A big (thrice) scatter in magnitude of A is conditioned, first, by different level of disturbances in different on-ground facilities and, second, by the fact that LTT depends on much more additional factors not considered in (1). The following values were used in [7]: $A = 200$ and $\beta = 0.2$ (hereafter, this correlation with these constants will be referred to as (1)). Close set of constants ($A = 200$ and $\beta = 0.187$) was proposed in [8]. Another set of constants $A = 275$ and $\beta = 0.134$ was proposed in [9] — correlation (1) with this set of constants will be referred hereafter as (1′).

The "Shuttle-like" criterion (see, e. g., [10, 11]) also belongs to this kind. It was widely used for transition onset prediction on the windward surface of the Space Shuttle. It has the following general form:

$$\frac{\mathrm{Re}_{\theta,\mathrm{tr}}}{\mathrm{M}_e} = B , \quad B = const . \tag{2}$$

This criterion has the same disadvantages as (1) and actually have to be applied only to a single object (Shuttle orbiter), but in practice, it was applied to wider range of reentry vehicles with sufficient success. For bluff bodies the constant of ≈ 270 is usually accepted but in case of sharp cones, more reliable data will be obtained with ≈ 100.

Other correlation for transition onset critical Reynolds number is [12]

$$\mathrm{Re}_{\theta,\mathrm{tr}} = 10.7 \left(\frac{\delta^*}{\theta}\right)^{0.34} \frac{\mathrm{Re}_1^{0.2}}{Z^{0.7}} \tag{3}$$

where $Z = \max\{1, k_w h_e/(\theta h_w)\}$ is the correction for surface roughness (h is the static enthalpy), and δ^* is the displacement thickness. Here, upstream flow prehistory is accounted for through the momentum thickness and boundary layer shape factor $H_{\mathrm{sf}} = \delta^*/\theta$. Relationship (3) can be used for a wide class of both sharp and blunted bodies, including the case of nonzero angles of attack.

Other dependence for transition onset critical Reynolds number for slender cones of similar type was introduced in [12, 13]:

$$\mathrm{Re}_{\theta,\mathrm{tr}} = A \left(1 + \frac{k_w}{\theta}\right)^{-0.65} \left(\frac{T_w}{T_0}\right)^{-0.7} \exp\left[0.114 \left(\mathrm{M}_e - 3.3\right)^2\right] \tag{4}$$

with $A = A_1/\mathrm{M}_\infty^{0.8}$ ($A_1 = const$ = 1400–1500 for wind tunnel conditions); T_w and T_0 are the wall and total temperatures; and M_∞ is the inflow Mach number. This formula explicitly accounts for the wall-to-stagnation temperature ratio T_w/T_0 effect on transition location and approximates nonmonotonic character of transition onset location depending on the outer edge Mach number; however, excessively strong dependence on M reduces its applicability to the range of $\mathrm{M} < 8$.

Criterion [14] was constructed exclusively for sharp cones and is a direct approximation of data from different test series. It was formulated on the basis of large series of on-ground tests both for wind tunnels and ballistic range experiments as well as available flight data. For on-ground test conditions, this correlation has the form

$$\mathrm{Re}_{x,\mathrm{tr}} = \mathrm{Re}_1^n \cdot 10^{C+Ds+Es^2} \tag{5}$$

with some set of empirical constants n, C, D, and

$$s = \mathrm{M}_e \left(\frac{h_w}{h_e}\right)^{0.7\exp(-0.05\mathrm{M}_e^2)} .$$

This expression is strictly local, that is, totally independent on the flow prehistory even by any integral boundary-layer thickness.

The simplest correlation of this kind used for sharp cones [15] has the form:

$$\mathrm{Re}_{s,\mathrm{tr}} = \begin{cases} 5 \cdot 10^5 , & \mathrm{M}_e < 1.4 ; \\ 2.42 \cdot 10^5 \mathrm{M}_e^{1.915} , & \mathrm{M}_e \geq 1.4 \end{cases} \tag{6}$$

where $\mathrm{Re}_{s,\mathrm{tr}}$ is the transition Reynolds number constructed from boundary layer outer edge parameters and cone tangent length.

A lot of correlations were developed for prediction of bypass transition induced by surface roughness. A governing parameter for these type of correlations is the characteristic roughness height k_w [16]. As an example, the newest relationships [17] are:

$$\left(\frac{\rho_e U_e \theta}{\mu_w}\right)_{\mathrm{tr}} = \begin{cases} 500 & \text{if } \dfrac{\rho_k U_k k_w}{\rho_e U_e \theta} \leq 0.5 \text{ — smooth wall asymptote for quite flow regime;} \\ 250 & \text{if } 0.5 \leq \dfrac{\rho_k U_k k_w}{\rho_e U_e \theta} \leq 2.5 \text{ — Reynolds number for critical roughness regime;} \\ 100 & \text{if } \dfrac{\rho_k U_k k_w}{\rho_e U_e \theta} \geq 2.5 \text{ — asymptotic regime for big roughness/low Reynolds number.} \end{cases} \tag{7}$$

In these expressions, values with subscript "k" are defined at the wall distance equal to roughness height.

There are different approaches to modeling transition region when transition onset location is already specified: linear-combination models, algebraic models, and differential models [18]. In differential models, transition is determined by governing differential equations connected to real physical processes; so, these models cannot be considered as empirical correlations (though large part of empirics is always present in those models). So, only first two groups for transition region models will be considered.

The linear-combination models are based on an assumption that the transitional flow is composed of intermittent spots of turbulence in an otherwise fully laminar flow. Under this assumption, the time-averaged flow field is a linear combination of the fully laminar and turbulent flows that originates where transition starts. The relative amounts of laminar and turbulent flow in the linear combination models are governed by the intermittency factor γ, which is defined as the fraction of time when the flow is turbulent. The most difficult aspect of this approach is determination of appropriate distribution for the intermittency. An important feature of this type of models is that it can be coupled with any method of calculating the laminar and turbulent flows. Pure laminar and turbulent flows around a body have to be calculated simultaneously when using these models. After that, these two flows are linearly mixed with the help of intermittency parameter. For example, heat flux distribution within the transition zone will be then

$$q_w = q_{w,\mathrm{lam}}(1-\gamma) + q_{w,\mathrm{tur}}\gamma\,. \tag{8}$$

Algebraic models were designed to be incorporated into turbulence models that use an eddy-viscosity assumption. They involve a modification of the effective viscosity, so that

$$\mu_{\mathrm{eff}} = \mu_{\mathrm{lam}} + \mu_{\mathrm{tur}}\gamma$$

where γ is the transition function equal to zero before the start of transition and equal to one at the end of transition zone. The use of algebraic models is convenient because these models involve very minor modifications to existing eddy-viscosity models.

It should be also realized that these two gammas (intermittency in linear-combination models and transition function in algebraic models) are actually different functions. But very often when using correlations, these two gammas are confused and the same formulas are used in both cases.

The simplest linear-combination transition region model was proposed in [19]:

$$\gamma = \begin{cases} 0\,, & Z \le 0; \\ 2Z^2\,, & 0 < Z \le 0.5\,; \\ 1 - 2(Z-1)^2\,, & 0.5 < Z \le 1\,; \\ 1\,, & Z > 1\,. \end{cases} \tag{9}$$

Here,

$$Z = \frac{\mathrm{Re}_\theta - \mathrm{Re}_\theta^-}{\mathrm{Re}_\theta^+ - \mathrm{Re}_\theta^-}\,; \qquad \mathrm{Re}_\theta^+ \approx \sqrt{2}\,\mathrm{Re}_\theta^-$$

where $\mathrm{Re}_\theta^{-/+}$ are the momentum thickness Reynolds numbers at transition start/finish.

The most known intermittency linear-combination model for transitional region based on Emmons turbulence spot theory is the model of Narasimha [20]. In this case, the intermittency can be found by the following expression:

$$\gamma = 1 - \exp\left(-0.411\left(\frac{x - x_{\mathrm{tr}}}{\lambda}\right)^2\right) \tag{10}$$

where x_{tr} is the coordinate of transition onset. Value of λ is defined to be the streamwise distance between the points where $\gamma = 0.25$ and $\gamma = 0.75$ and can be determined by relations described in [20]. Extended review of such models (more than ten ones) is presented in [21].

One of the most well-known and often used models of this kind is a model [22]

$$\gamma = 1 - \exp\left(Gr_0\left(x_{\mathrm{tr}}\right)\left(\int\limits_{x_{\mathrm{tr}}}^{x}\frac{dx}{r_0}\right)\left(\int\limits_{x_{\mathrm{tr}}}^{x}\frac{dx}{U_e}\right)\right) \tag{11}$$

where

$$G = 8.33 \cdot 10^{-4}\,\frac{U_e^3}{\nu_e^2}\,\mathrm{Re}_{x_{\mathrm{tr}}}^{-1.34}$$

and $r_0(x)$ is the body radius.

Among multitude of algebraic models for transition zone only one correlation will be considered [23] that has the following form:

$$\gamma = \begin{cases} 1 - \exp\left\{-4.5\left[\chi\left(1 + 0.02\mathrm{M}_e^2\right) - 0.005\mathrm{M}_e^2\right]^2\right\}, & 0 \le \chi < 0.25\,; \\ 18.628\chi^4 - 55.388\chi^3 + 52.369\chi^2 & \\ \qquad - 16.501\chi + 1.893\,, & 0.25 \le \chi < 0.75\,; \\ 1.25 - 0.25\sin\left[\pi\left(0.444\chi - 0.833\right)\right], & 0.75 \le \chi < 3\,; \\ 1\,, & \chi > 3 \end{cases} \tag{12}$$

where

$$\chi = \frac{\theta/\theta_{\mathrm{tr}} - 1 + 0.005\mathrm{M}_e^2}{1 + 0.02\mathrm{M}_e^2}\,.$$

This model is governed by the only parameter (χ) that increases with momentum thickness growth. As it can be seen, the maximum value of $\gamma = 1.5$ is achieved at $\chi = 0.75$. It means that in this case, transition function cannot be considered as the intermittency. It can be clearly seen by the fact that it reaches

the values above unity while the intermittency is bounded between zero and unity. This overshoot above unity is an attempt to model the peak above the nominal turbulent value in skin friction and heat transfer at the end of transition zone.

One principal disadvantage of all these methods is a complexity of their use together with modern CFD methods based on RANS equations as they require boundary layer thickness and edge parameters to be specified that can be nontrivial problem for real supersonic flows. One way of ruling out this disadvantage is presented in the next section.

3 TRANSITION PREDICTION USING REYNOLDS-AVERAGED NAVIER–STOKES EQUATIONS

Another way of LTT prediction, actually very close to the correlation approaches of previous section, is using RANS equations with some two-equation differential model for turbulent viscosity and additional equation(s) for description of flow transition. The most known of them is Langtry–Menter transition model [4] used together with k–ω SST model of Menter [5]. In reality, most of differential turbulence models (including k–ω SST) suffer from early transition and some special procedure is required for transition delay for higher Reynolds numbers. In [5], for account of LTT, the term with turbulence production in equation for turbulent kinetic energy k is multiplied to the intermittency function γ (also, dissipation term is slightly modified) in hope that this term will be switched on only at actual transition start. In this case, γ depends on not only longitudinal coordinate but is distributed within the flowfield. Nevertheless, this value is some analogue of the intermittency coefficient used in algebraic correlations. Intermittency equation [4] has the form:

$$\frac{\partial(\rho\gamma)}{\partial t} + \frac{\partial(\rho\gamma u_i)}{\partial x_i} = \left[\frac{\partial}{\partial x_j}\left(\mu_l + \frac{\mu_t}{\sigma_k}\right)\frac{\partial\gamma}{\partial x_j}\right] + P_\gamma - E_\gamma \tag{13}$$

where term with γ production is

$$P_\gamma = F_{\text{length}} c_{a1} \rho S \sqrt{\gamma F_{\text{onset}}}\,(1 - c_{e1}\gamma)\ .$$

Here, S is the shear stress intensity. Production term has to be equal to zero in laminar flow that is reached by multiplication to F_{onset} correlation function. Intensity of γ production and, consequently, extensions of LTT zone are regulated by a coefficient F_{length}. The last (bracketed) term in this expression is introduced to limit the value of γ by one. Here and hereafter, the following notations are used: y — distance from a wall; Re_v — vorticity Reynolds number:

$$\mathrm{Re}_v = \frac{\rho y^2 S}{\mu};$$

R_T — turbulent Reynolds number:

$$R_T = \frac{\rho k}{\mu\omega};$$

$$F_{\mathrm{onset1}} = \frac{\mathrm{Re}_v}{2.193\mathrm{Re}_{\theta,c}}; \qquad F_{\mathrm{onset2}} = \min\left(\max\left(F_{\mathrm{onset1}}, F_{\mathrm{onset1}}^4\right), 2.0\right); \quad (14)$$

$$F_{\mathrm{onset3}} = \max\left(1 - \left(\frac{R_T}{2.5}\right)^3, 0\right); \qquad F_{\mathrm{onset}} = \max\left(F_{\mathrm{onset2}} - F_{\mathrm{onset3}}, 0\right)$$

where $\mathrm{Re}_{\theta,c}$ parameter in these expressions is the critical momentum thickness Reynolds number at which intermittency starts to appear in the boundary layer.

Intermittency destruction term in (13) is

$$E_\gamma = c_{a2}\rho\Omega\gamma F_{\mathrm{turb}}\left(c_{e2}\gamma - 1\right)$$

where Ω is the local value of flow vorticity. This term provides lack of intermittency in laminar flow as well as modeling of flow relaminarization under strong favorable pressure gradient. Here, the following correlation function is used:

$$F_{\mathrm{turb}} = \exp\left(-\left(\frac{R_T}{4}\right)^4\right) \quad (15)$$

Second additional equation of the model [4] is written for value of critical Re_θ at transition. This value, distinguishing of usual approaches, is considered to be variable across the boundary layer. Transport equation for this value is written as [4]

$$\frac{\partial(\rho\mathrm{Re}_{\theta,t})}{\partial t} + \frac{\partial(\rho\mathrm{Re}_{\theta,t}u_i)}{\partial x_i} = \frac{\partial}{\partial x_j}\left[\sigma_k\left(\mu_l + \mu_t\right)\frac{\partial\mathrm{Re}_{\theta,t}}{\partial x_j}\right] + P_{\theta t} \quad (16)$$

with the source term

$$P_{\theta t} = c_{\theta t}\frac{\rho}{t}\left(\mathrm{Re}_{\theta,\mathrm{tr}} - \mathrm{Re}_{\theta,t}\right)\left(1 - F_{\theta t}\right)$$

and $t = 5000\mu/(\rho U^2)$. The $F_{\theta t}$ function is equal to zero in inflow and tends to unity within the boundary layer.

Thus, transition model [4] is devised by the following manner — LTT onset location is determined from Eq. (16) for $\mathrm{Re}_{\theta,t}$ function with the boundary condition $\mathrm{Re}_{\theta,t} = \mathrm{Re}_{\theta,\mathrm{tr}}$ at the outer edge. Here, $\mathrm{Re}_{\theta,\mathrm{tr}}$ is the usual transition onset critical Reynolds number, determined from some correlation. It means that actual transitional Reynolds number $\mathrm{Re}_{\theta,\mathrm{tr}}$ has to be known before any

calculations. As such the correlation of form $\mathrm{Re}_{\theta,\mathrm{tr}}(\mathrm{Tu})$ like that of [24, 25] is used in [4] though any other correlation like (1)–(4) can be equally used. Main difficulty in using these correlations together with RANS is requirement for explicit boundary layer allocation that can be rather inconvenient. In model [4], critical Reynolds number depends mainly on explicitly given inflow velocity disturbance level Tu, though in practice, it is seldom known with required accuracy.

Then value of $\mathrm{Re}_{\theta,t}$ is transported from the outer edge of computational zone according to convection-diffusion equation (16). In the inflow, the production source term $P_{\theta,t}$ is positive when $\mathrm{Re}_{\theta,t} > \mathrm{Re}_{\theta,\mathrm{tr}}$ and negative otherwise that, in turn, leads to production/decay of $\mathrm{Re}_{\theta,t}$ in inflow. Within the boundary layer, source term in (16) tends to zero, that is, there is simple diffusion of $\mathrm{Re}_{\theta,t}$ from the boundary-layer outer edge toward the wall.

Transition will be developed when $\mathrm{Re}_{\theta,c}$ in (14) reaches its critical magnitude. Since $\mathrm{Re}_{\theta,c}$ is the value of Re_{θ} for which intermittency starts to appear in the boundary layer, then some distance downstream is required for that the intermittency origination affects the velocity profile and always $\mathrm{Re}_{\theta,c} < \mathrm{Re}_{\theta,\mathrm{tr}}$. These two values are again connected by some correlation of type $\mathrm{Re}_{\theta,c} = F(\mathrm{Re}_{\theta,\mathrm{tr}})$. When in the boundary layer value of $\mathrm{Re}_{\theta,t}$ becomes greater than $\mathrm{Re}_{\theta,c}$, then positive source in Eq. (13) for intermittency γ "switches on" at that point and γ starts growing (and turbulent kinetic energy starts increasing together with it) and transition begins. As it follows from (14), intermittency starts to grow at that point within the boundary layer where function $\mathrm{Re}_v/\mathrm{Re}_{\theta}$ reaches its maximum according to VanDriest–Blumer model [26].

Main advantage of the transition model [4] is simplicity of its incorporation into existing RANS numerical codes that cannot be told about algebraic correlations of form (1)–(7). On the other hand, model [4] has some disadvantage that hampers its use, especially for flows with high Mach numbers. The reason is that this model was originally developed for modeling internal turbomachinery flows characterized by rather moderate compressibility that strongly distincts them from super/hypersonic external flows. Mainly, it is stipulated by essential difference of boundary-layer profiles in compressible boundary layer from those in incompressible case. This discrepancy can be partly eliminated if boundary layer parameters will be redefined in new variables like that of Lees–Dorodnitsyn; however, using such variables in modern RANS codes is complicated and making this coordinate transformation totally to depreciate main advantages of the method.

As it is indicated in [4], VanDriest–Blumer parameter [26]

$$\mathrm{VDB}_{\max} = \frac{\max(\mathrm{Re}_v)}{2.193\mathrm{Re}_{\theta}}$$

is a weakly changing function (within the range 0.95–1.4) of boundary layer shape factor $H_{\mathrm{sf}} = \delta^*/\theta$ that also changes only slightly (for flows considered

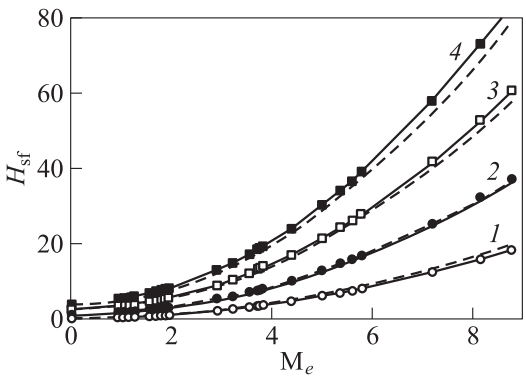

Figure 1 Variation of boundary layer shape factor $H_{sf} = \delta^*/\theta$ depending on outer edge Mach number at different values of temperature ratios: *1* — $t_w = 0.1$; *2* — 0.5; *3* — 1.0; and *4* — $t_w = 1.5$. Dashed curves refer to Eq. (17) and the signs to Eq. (18)

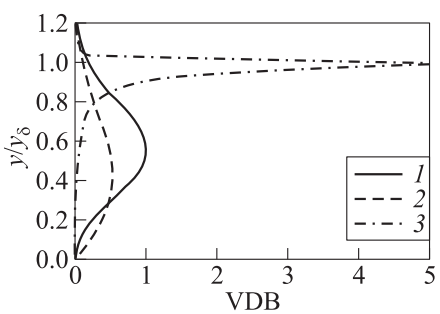

Figure 2 Comparison of VanDriest–Blumer functions across the boundary layer for Blasius (*1*) and compressible flows: *2* —$M_e = 1.26$, $t_w = 0.1$; and *3* —$M_e = 8.77$, $t_w = 1.0$

in [4]): $-2.2 < H_{sf} < 3.6$ near the value specific for Blasius profile $H_{sf} = 2.59$ and depends, mainly, on pressure gradient. For supersonic and hypersonic flows, this situation changes drastically. In this case, both boundary-layer shape factor and VanDriest–Blumer parameters are the strong functions of outer edge Mach number (M) and wall-to-stagnation temperature ratio ($t_w = T_w/T_0$) (Figs. 1 and 2).

As it follows from Fig. 1, value of shape factor for supersonic boundary layers can vary within very wide limits (from low negative values at low M and t_w to very high at large values of these parameters). Form of VanDriest–Blumer function VDB $(y) = \mathrm{Re}_v/(2.193\mathrm{Re}_\theta)$ and position and magnitude of its maximum strongly changes compared to incompressible case (see Fig. 2). This circumstance

leads to the fact that when using function F_{onset1} in (14), the intermittency generation in the boundary layer and following transition start at the points either upstream or downstream of the actual regions where momentum thickness Reynolds number achieves its critical value $\text{Re}_{\theta,c}$.

For locally self-similar boundary layer, the value of shape factor can be estimated as

$$H_{\text{sf}} = \frac{\delta^*}{\vartheta} = 2.59\,\frac{h_w}{h_e} + 0.2\text{M}_e^2 = 2.59 t_w\left(1 + 0.2\text{M}_e^2\right) + 0.2\text{M}_e^2\,. \tag{17}$$

This dependence is shown in Fig. 1 with dashed curves. For flows with sufficiently weak effect of pressure gradient, even more accurate (with uncertainty $< 5\%$) formula was obtained in the present work (within the range $0.05 < t_w < 2$, $\text{M}_e < 12$) (signs in Fig. 1):

$$H_{\text{sf}} \approx (0.5741 t_w + 0.1794)\,\text{M}_e^2 + 2.872 t_w - 0.2667\,. \tag{18}$$

In this case, for estimation of Mach number at the boundary-layer, outer edge Mach number value at $y = 2y_{\max}$ can be employed, where $y_{\max}$ is the distance from the wall, where maximum of vorticity function $\text{VDB}\,(y)$ is achieved.

For the same conditions, the following approximation (with uncertainty $< 10\%$) for VanDriest–Blumer parameter was obtained:

$$\text{VDB}_{\max} = \text{VDB}\,(y_{\max}) = \frac{\max(\text{Re}_v)}{2.193\text{Re}_\theta} \approx (0.07 H_{\text{sf}} + 0.9)\,t_w^{-0.2}\,. \tag{19}$$

Then modified expression for specification of location intermittency growth onset can be written as

$$F_{\text{onset 1}} = \frac{\text{Re}_v}{2.193\text{VDB}_{\max}\text{Re}_{\theta,c}}\,. \tag{20}$$

Another approach for accounting of compressibility effect on position and size of transition zone is using empirical corrections [27]:

$$\text{Re}_{\theta,c} = \text{Re}_{\theta,c,\text{incompr}}\sqrt{1 + 0.3\text{M}_e^{0.6}}\,; \quad F_{\text{length}} = \frac{F_{\text{length,incompr}}}{1 + 0.25\text{M}_e^{0.625}}\,.$$

Transition criterion used in [4] in the form of critical Reynolds number $\text{Re}_{\theta,\text{tr}}$ dependence on inflow disturbance level Tu is a generalization of empirical data for sufficiently weakly-compressible flows and similar to well-known criterion of [24, 25]. For conditions specific for the turbomachinery internal flows, the inflow disturbance level is usually quite high ($\sim 10\%$) and in that case, dependence of $\text{Re}_{\theta,\text{tr}}$ on Tu appears to be rather slight (Fig. 3). For flows in common (nonquiet) hypersonic aerodynamic wind-tunnels value of Tu $\sim 1\%$ and one comes to the region of strong dependence of $\text{Re}_{\theta,\text{tr}}(\text{Tu})$. Exact value of inflow disturbance in common facilities for each certain experiment is rarely known and

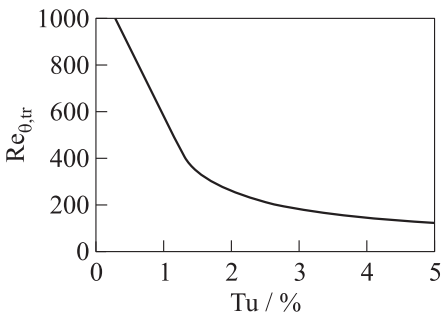

Figure 3 Dependence $\mathrm{Re}_{\theta,\mathrm{tr}}$ vs. Tu

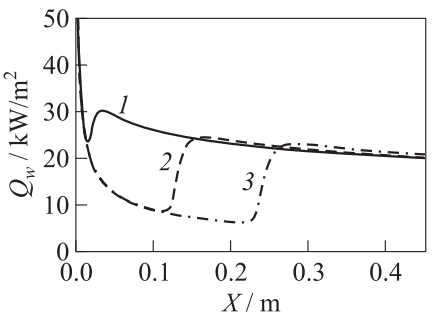

Figure 4 Influence of Tu on transition calculated with γ–Re_θ model: *1* — Tu = 1.5%; *2* — 1.0%; and *3* — Tu = 0.5%

quite acceptable variation of inflow disturbance in ±0.5% relative to level of 1% brings about very strong variation in transition onset location (Fig. 4). In simple situations (flat plate, wedge or cone flow) when boundary-layer outer edge Mach number is known *a priori*, the simplest correlations like (1)–(4) can be used for specification of $\mathrm{Re}_{\theta,\mathrm{tr}}$ instead of $\mathrm{Re}_{\theta,\mathrm{tr}}(\mathrm{Tu})$ dependence of Fig. 3. However, the accuracy of these criteria is also insufficient that will be demonstrated below.

One more disadvantage of the model [4] used for hypersonic flows is its excessive damping of turbulence production within the near-wall region in some cases. In these situations, transition stalls at once after its start. First of all, this damping is produced by the F_{turb} term (15) that provides intensive decrease of the turbulent intermittency near the wall. It follows from the form of this term that there is no generation of intermittency in the near-wall region where $R_t \le a$ (R_t is the turbulent Reynolds number: $R_t = \mu_{\mathrm{tur}}/\mu_{\mathrm{tam}}$ and a is the empirical constant accepted to be equal to 4 in (15)). This value of the parameter a turns to be excessively restricting for strongly compressible hypersonic flows and region with $R_t \le 4$ can embrace considerable part of the boundary layer depending on Mach number, wall temperature, and Reynolds number magnitudes. Especially, it may concern transition region where virtual profile of turbulent viscosity is still under development. Therefore, to get actual transition in supersonic flow, it was necessary to reduce value of a parameter shrinking, thereby, near-wall region for intermittency damping.

At nominal value of parameter $a = 4$, intermittency quickly becomes "frozen" at value $\gamma \approx 0.2$ soon after transition start and practically does not grow (Fig. 5). At value $a = 1$, LTT starts somewhat upstream than at $a = 4$ and intermittency grows almost to the turbulent level but then stales again at $\gamma \approx 0.9$. Only at $a \approx 0.25$, transition comes to its finishing state with $\gamma = 1$ asymptotically

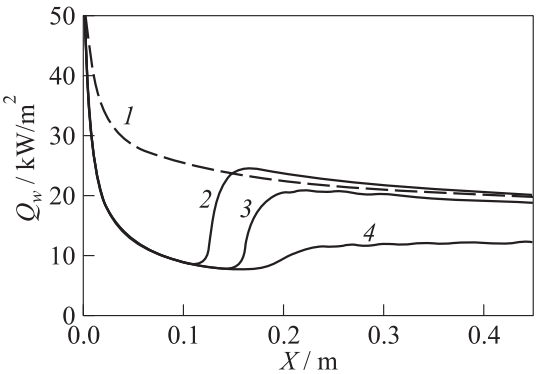

Figure 5 Influence of constant a of the γ–Re_θ model on LTT. $\mathrm{M}_\infty = 6.2$; $\mathrm{Re}_{\infty,1} = 2.91 \cdot 10^7$; $t_w = 0.6\%$; 7 degree cone; $\mathrm{Tu} = 1\%$; $\mathrm{Re}_{\theta,\mathrm{tr}} = 584$; and $F_{\mathrm{turb}} = \exp\left(-(R_t/a)^4\right)$: *1* — k–ω SST; *2* — $a = 0.25$; *3* — 1; and *4* — $a = 4$

approaching the turbulent flow values (dashed line in Fig. 5). Therefore, all calculations of supersonic flows using RANS were made with just this value of constant a.

4 RESULTS OF LAMINAR–TURBULENT TRANSITION MODELING ON CONES IN SUPERSONIC FLOW USING ENGINEERING CORRELATIONS AND REYNOLDS-AVERAGED NAVIER–STOKES EQUATIONS

Results of analysis above were used for modeling laminar–turbulent transition on 7 degree cones in supersonic ($\mathrm{M} \approx 6$) air flow at zero angle of attack by means of engineering correlations and RANS within the framework of FP7 TransHyBeriAN project [3]. Possibility of LTT control by local heating/cooling was studied within this work by both experimental and numerical methods. Correlation predictions of transition on cones were made by integration of the boundary layer equations with Sebeci–Smith eddy viscosity algebraic model [22]. Reynolds averaged equations were solved using full Navier–Stokes equations with k–ω SST [5] differential model for turbulent viscosity.

Modeling of the transition zone with (9)–(12) correlations does not cause serious difficulties if the transition onset is already determined. Figure 6 demonstrates comparison of results for transition zone modeling using different correlations (9)–(12) both linear-combination and algebraic ones.

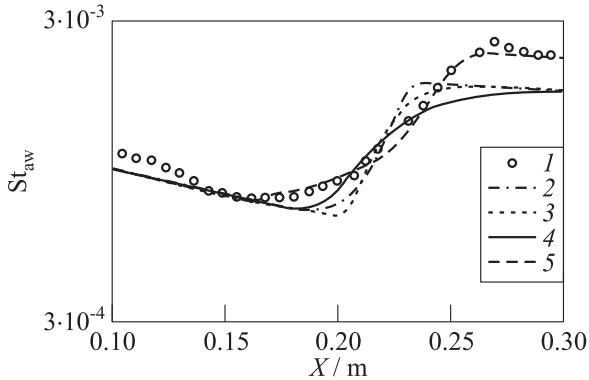

Figure 6 Comparison of different correlations for transition zone modeling; $P_0 = 3.58 \times 10^6$ Pa; $T_0 = 597$ K; and $\mathrm{Re}_u = 24.53 \cdot 10^6$: *1* — experiments [28]; *2* — correlation (9); *3* — (10); *4* — (11); and *5* — correlation (12)

In these calculations, the transition onset location was selected artificially for better agreement with the test data [28]. It may be concluded that all these correlations provide admissible behavior of the heat flux within the transition region. However, different positions of transition start have to be assigned for each correlation of (9)–(12) for better accordance with the test data. Thus, the transition onset was located at $x = 0.186$ m for correlation (11), at $x = 0.175$ m for (9), at $x = 0.19$ m for (10), and at $x = 0.165$ m for correlation (12).

The latest correlation provides the best results compared to others reproducing test results in the most adequate manner as concerns transition zone size and heat flux distribution for different parts of transition zone — initial region of nonlinear growth of disturbances and heat flux overshoot in the end of transition zone.

Situation with prediction of the transition onset using engineering correlations is much worse (Table 1).

Error values for transition onset predictions for sharp slender cones with correlations (1)–(7) are presented in Table 1 for a number of known experimental results. In some cases (emdash signs in the table), there was no transition observed at any reasonable distance. Correlations (1) and (1′) provide earlier transition except for cold wall cases ($t_w = T_w/T_0 \leq 0.1$). Correlation (2) (with the constant $B = 100$) also gives earlier transition for on-ground test conditions but for free-flight [40], transition turns to be very far upstream (up to 6-times further). Correlations (3) and (5) provide surprisingly close onset locations for tests in aerodynamic facilities with short lagging compared to experiments but for flight conditions approximation (5) gives considerably larger deviation from the experiments. Correlation (4) is applicable only for moderate Mach numbers

Table 1 Accuracy of transition onset predictions for correlations (1)–(7)

Ref.	θ_c°	t_w	M_e	x_{tr}, m (exp.)	$Re_{e,1}$	$Re_{\theta,tr}$	Error*, %							
							(1)	(1′)	(2)	(3)	(4)	(5)	(6)	(7)
[28]	10	0.52	5.5	0.29	$9.7 \cdot 10^6$	618	2	−7	−20	28	122	25	126	
[28]	10	0.53	5.5	0.25	$1.1 \cdot 10^7$	607	2	−6	−17	39	117	35	129	
[28]	10	0.53	5.5	0.24	$1.3 \cdot 10^7$	636	−6	−13	−24	34	96	30	106	
[28]	10	0.52	5.6	0.25	$1.4 \cdot 10^7$	671	−12	−20	−31	24	75	20	92	
[28]	10	0.52	5.6	0.20	$1.7 \cdot 10^7$	663	−10	−18	−29	38	82	33	95	
[28]	10	0.52	5.6	0.19	$1.9 \cdot 10^7$	693	−14	−22	−35	35	68	30	84	
[28]	10	0.52	5.6	0.19	$2.1 \cdot 10^7$	726	−22	−30	−41	27	48	22	65	
[28]	10	0.52	5.6	0.17	$2.2 \cdot 10^7$	700	−18	−24	−36	39	68	33	76	
[28]	10	0.52	5.6	0.17	$2.4 \cdot 10^7$	723	−21	−27	−40	36	58	27	64	
[28]	10	0.52	5.6	0.17	$2.6 \cdot 10^7$	751	−24	−33	−45	30	48	24	55	
[28]	10	0.53	5.6	0.17	$2.9 \cdot 10^7$	806	−36	−39	−52	21	23	12	33	
[28]	10	0.47	5.6	0.25	$1.2 \cdot 10^7$	620	2	−8	−19	31	143	29	120	
[28]	10	0.47	5.6	0.24	$1.4 \cdot 10^7$	665	−11	−19	−30	23	114	19	91	
[28]	10	0.46	5.6	0.22	$1.7 \cdot 10^7$	689	−16	−23	−34	21	102	19	77	
[28]	10	0.46	5.6	0.20	$1.9 \cdot 10^7$	701	−18	−26	−36	26	101	21	72	
[28]	10	0.45	5.6	0.17	$2.2 \cdot 10^7$	687	−12	−21	−34	36	115	30	79	
[29]	7	0.07	8.1	0.98	$4.3 \cdot 10^6$	656	135	54	52	−28	2378	−17	215	
[29]	7	0.07	8.1	1.24	$3.2 \cdot 10^6$	644	149	61	60	−32	2682	−22	229	
[30]	5	0.59	5.5	0.55	$4.4 \cdot 10^6$	574	12	3	−8	10	140	8	166	
[30]	5	0.59	5.5	0.32	$1.1 \cdot 10^7$	683	−17	−25	−35	13	81	10	87	
[30]	5	0.59	5.6	0.20	$1.7 \cdot 10^7$	671	−10	−18	−31	44	85	36	100	
[30]	5	0.59	5.6	0.15	$2.3 \cdot 10^7$	693	−13	−20	−35	57	87	47	87	
[31]	7	0.42	6.8	0.36	$9.1 \cdot 10^6$	660	41	10	6	25	852	21	187	
[32]	10	0.60	5.0	0.19	$4.6 \cdot 10^7$	1078	−68	−68	−79	−24	−57	−27	−38	
[33]	7.5	0.53	5.4	0.35	$8.0 \cdot 10^6$	614	−9	−13	−23	13	94	11	109	
[33]	7.5	0.53	5.4	0.16	$2.2 \cdot 10^7$	693	−27	−31	−40	33	53	33	64	
[33]	7.5	0.53	5.4	0.09	$4.3 \cdot 10^7$	720	−28	−33	−44	61	44	58	53	
[33]	7.5	0.53	5.4	0.07	$6.5 \cdot 10^7$	752	−37	−42	−49	71	31	71	40	
[33]	7.5	0.53	5.4	0.05	$8.8 \cdot 10^7$	767	−38	−42	−51	86	28	86	34	
[33]	7.5	0.53	5.4	0.04	$1.3 \cdot 10^8$	781	−37	−43	−52	111	26	111	31	
[34]	5	0.27	8.8	0.44	$9.0 \cdot 10^6$	725	166	59	46	30	—	66	291	
[35]	8	0.27	4.9	0.43	$7.0 \cdot 10^6$	616	−24	−24	−38	−27	296	−8	66	
[35]	8	0.29	4.9	0.25	$1.4 \cdot 10^7$	663	−33	−33	−46	−15	210	3	43	
[35]	8	0.52	4.9	0.37	$1.9 \cdot 10^7$	965	−66	−66	−75	−42	−32	−39	−28	
[35]	8	0.44	4.9	0.33	$1.6 \cdot 10^7$	833	−56	−56	−66	−32	12	−26	−6	
[35]	8	0.21	4.9	0.38	$6.8 \cdot 10^6$	572	−12	−12	−28	−24	551	6	91	
[35]	8	0.16	4.9	0.18	$1.6 \cdot 10^7$	584	−17	−19	−30	−8	744	36	69	
[35]	8	0.38	4.9	0.57	$8.8 \cdot 10^6$	801	−54	−55	−63	−46	46	−39	0	
[36]	5	0.21	10.2	1.22	$4.9 \cdot 10^6$	868	213	55	38	−24	—	66	242	

(*Continued*)

Table 1 Accuracy of transition onset predictions for correlations (1)–(7) (*Continued*)

Ref.	θ_c°	t_w	M_e	x_{tr}, m (exp.)	$Re_{e,1}$	$Re_{\theta,tr}$	Error*, %							
							(1)	(1′)	(2)	(3)	(4)	(5)	(6)	(7)
[37]	5	0.40	4.2	0.07	$1.2 \cdot 10^8$	1023	−76	−74	−83	−21	−16	9	−53	
[37]	5	0.40	4.3	0.12	$3.7 \cdot 10^7$	748	−59	−55	−67	−6	53	26	−9	
[38]	10	0.17	4.4	0.17	$1.2 \cdot 10^8$	1619	−90	−89	−93	−75	−7	−52	−80	
[38]	10	0.17	4.4	0.06	$3.2 \cdot 10^8$	1613	−87	−87	−93	−62	−3	−29	−79	
[39]	5	0.12	5.6	0.06	$8.7 \cdot 10^7$	781	−34	−40	−49	17	1159	50	29	
[40]	5	0.02	15.1	2.93	$1.5 \cdot 10^7$	888	554	71	189	−56	—	481	9	−86
[40]	5	0.02	15.1	2.84	$1.6 \cdot 10^7$	903	499	55	180	−60	—	407	1	−90
[40]	5	0.02	15.1	2.74	$1.8 \cdot 10^7$	916	452	44	170	−62	—	398	−5	−91
[40]	5	0.02	15.0	2.44	$1.9 \cdot 10^7$	931	454	45	159	−59	—	432	−3	−91
[40]	5	0.02	15.0	2.38	$2.1 \cdot 10^7$	943	406	33	152	−61	—	417	−10	−91
[40]	5	0.02	14.9	2.32	$2.3 \cdot 10^7$	984	360	22	129	−63	—	403	−17	−92
[40]	5	0.02	14.8	2.26	$2.5 \cdot 10^7$	1000	317	12	120	−64	—	385	−23	−92
[40]	5	0.02	14.7	2.23	$2.7 \cdot 10^7$	1036	269	0	102	−66	—	360	−29	−93
[40]	5	0.02	14.6	2.16	$2.9 \cdot 10^7$	1039	227	−10	98	−67	—	336	−35	−93
[40]	5	0.02	14.5	2.07	$3.1 \cdot 10^7$	1059	199	−17	88	−68	—	326	−38	−93
[40]	5	0.02	14.4	2.01	$3.4 \cdot 10^7$	1107	172	−23	70	−69	—	312	−42	−94
[40]	5	0.02	14.0	1.68	$3.5 \cdot 10^7$	1055	155	−23	76	−66	—	318	−36	−93
[40]	5	0.03	13.8	1.62	$3.5 \cdot 10^7$	1017	126	−30	83	−67	—	295	−40	−93
[40]	5	0.03	13.2	1.40	$3.4 \cdot 10^7$	909	99	−34	112	−65	—	278	−37	−92
[40]	5	0.03	12.9	1.34	$3.5 \cdot 10^7$	934	76	−39	92	−66	—	255	−39	−92
[40]	5	0.04	12.4	1.22	$3.4 \cdot 10^7$	882	47	−45	98	−66	—	224	−40	−91
[40]	5	0.05	11.0	0.93	$2.4 \cdot 10^7$	627	13	−49	208	−62	—	193	−29	−87
[40]	5	0.06	10.4	0.87	$2.2 \cdot 10^7$	590	−6	−54	211	−62	—	157	−31	−83
[40]	5	0.07	10.2	0.85	$2.2 \cdot 10^7$	601	−13	−57	188	−62	—	142	−33	−81
[40]	5	0.09	9.7	0.81	$2.0 \cdot 10^7$	601	−22	−59	161	−60	—	117	−33	−74
[40]	5	0.16	8.8	0.69	$1.5 \cdot 10^7$	546	−32	−59	157	−53	—	79	−29	−49
[40]	5	0.44	6.2	0.43	$5.2 \cdot 10^6$	234	−44	−53	595	−22	135	87	−11	82
Average error, %							59	−20	29	−11	257	111	42	−80
Standard deviation, %							155	36	113	48	562	148	80	38

*Error $= (x_{tr,\,corr} - x_{tr,exp})/x_{tr,exp} \cdot 100\%$

Remarks: white cells — tests in wind and shock tunnels; light-grey — tests in ballistic ranges; and dark-grey — free-flight data.

and for all cases with $M > 7$, too big error occurred. Correlation (6) leads to significant spread for on-ground test conditions but flight data are described quite satisfied. Correlation (8) is practically nonapplicable for cold supersonic on-ground tests and since this correlation, first of all, is governed by the surface roughness value (unknown for the most experiments), then its output is presented only for the flight test data assuming characteristic roughness of $k_w = 1$ μm. As a whole, one can infer that correlations provide sufficiently reliable results only

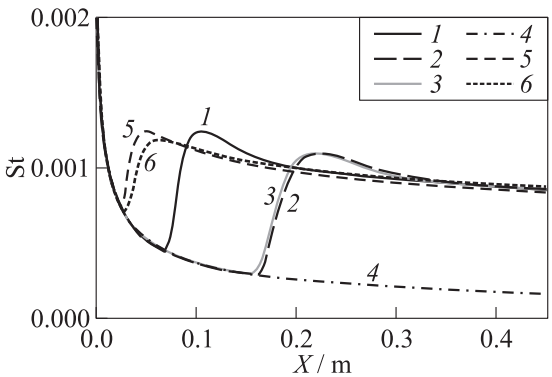

Figure 7 Laminar–turbulent transition modeling for 7 degree sharp cone at M = 6, $\mathrm{Re}_1 = 28 \cdot 10^6$, $T_w = const = 295$ K: *1* — correlation (1); *2* — (3); *3* — correlation (5); *4* — laminar; *5* — RANS, $a = 0.25$; *6* — RANS, $a = 0.25$ and correlation (20)

for flow conditions close to conditions for which they were obtained. Predictive capability of these criteria is insufficient. Better correspondence with the test data was demonstrated for the correlations of (1′) and (3).

Stanton number ($\mathrm{St} = q_w/(\rho_\infty U_\infty (H_0 - h_w))$) distribution along the axis of sharp 7 degree cone at M = 6, $\mathrm{Re}_1 = 28 \cdot 10^6$, and $T_w = const = 295$ K calculated with correlations (1), (3), and (5) and RANS (with and without correction of (20)) at fixed value of Tu = 1% is shown in Fig. 7. In this case, magnitude of $\mathrm{VDB}_{\max}$ parameter (19) is occasionally close to 1 and transition onset locations calculated with and without correction (20) are very close. At inflow disturbance value of 1% (accepted in calculations), the LTT started well upstream compared to results of correlations.

When the cone is equipped with heated/cooled insert (as it is shown in bottom part of Fig. 8), there will be local supply/sink of thermal energy to the boundary layer on the cone. This supply/sink is able to affect transition onset location. General mechanism of this displacement is variation of the boundary layer receptivity to external disturbances due to abrupt change of boundary layer thickness in the vicinity of the insert. But this variation in receptivity cannot be described by averaged Navier–Stokes equations as well as by the correlations such as (1)–(7). Mechanisms affecting the boundary layer transition in this case are: (*i*) straightforward effect of temperature ratio variation ($t_w = T_w/T_a$ where T_a is the recovery temperature) for those correlations that depends on it by explicit (or indirect) manner (correlations (3)–(7)); and (*ii*) indirect influence because of variation of momentum thickness for correlations of (1)–(4), (7), and (20). The latest effect is not very pronounced as momentum thickness grows continuously and changes only weakly at wall temperature variation. It follows from integral

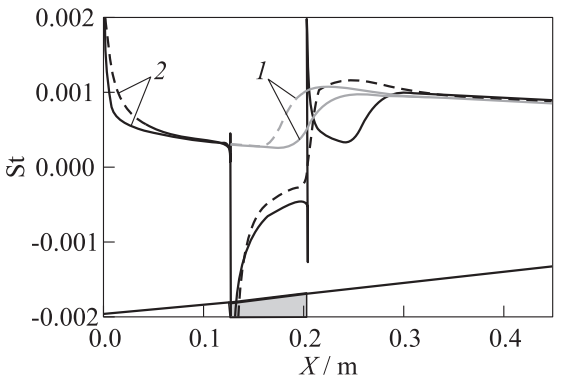

Figure 8 Effect of local heating on LTT for blunted ($R_N = 1.5$ mm) 7 degree cone at M = 6 and $\mathrm{Re}_1 = 28 \cdot 10^6$: *1* — no temperature step; *2* — $t_w = 1.0$; solid curves refer to RANS; and dashed curves refer to boundary layer equations

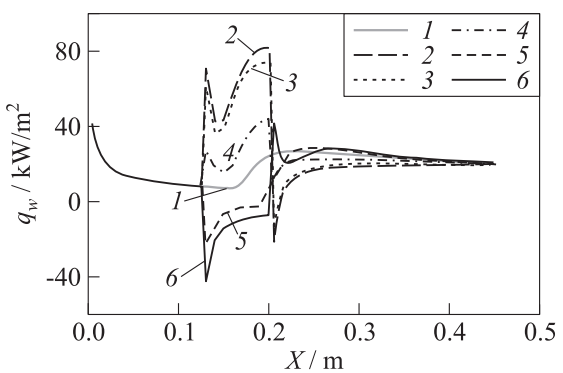

Figure 9 Effect of local heating/cooling on LTT for 7 degree sharp cone at M = 6 and $\mathrm{Re}_1 = 28 \cdot 10^6$: *1* — baseline; *2* — $t_w = 0.1$; *3* — 0.2; *4* — 0.5; *5* — 1.0; and *6* — $t_w = 1.2$

momentum equation for gradientless flow $d\theta/dx = c_f/2$ where c_f is the skin friction coefficient that changes rather slightly with wall temperature jump.

For all correlations under consideration, influence of local heating/cooling on location of transition onset was not very significant but it always leads to the same effect: heating led to downstream displacement of the LTT onset whereas cooling — to upstream displacement. The most explicit effect of this displacement is demonstrated when using correlation (3) (Fig. 9). As it was expected, very strong dependence of the LTT onset on wall temperature jump was observed for criterion of (7). At given value of surface roughness, there was no

transition in most cases, but at the lowest values of wall temperature ($t_w \leq 0.2$) with corresponding abrupt grows of ρ_k, the flow was triggered from smooth wall to the critical roughness regime and transition starts.

For the flow regime considered here ($M = 6$ and $Re_1 = 28 \cdot 10^6$), transition onset on sharp cone takes place sufficiently early (at the insert or even before it). In order to move transition start downstream, a cone with small nose bluntness $R_N = 1.5$ mm was considered. It allows remarkable displacing transition zone downstream compared to the sharp cone case (see Fig. 7). Effect of local heating on transition start point for slightly blunted cone is presented in Fig. 8 for numerical modeling of boundary layer equations with correlation (3) and by RANS integration using model [4]. In both cases, enlarging of the laminar zone at local wall heating on the insert was obtained (the insert temperature was equal to the flow recovery temperature T_a and other cone parts had constant wall temperatures of $0.7T_a$). It is seen that use of RANS equation with the transition model [4] leads to greater displacement of the transition downstream than in the case of correlations. This effect is explained by appearance of additional effects of viscous–inviscid interaction in the vicinity of temperature jump and rise of induced pressure gradient.

5 CONCLUDING REMARKS

Different engineering algebraic correlations for numerical modeling of transitional flows on sharp cones in hypersonic flows both for transition onset prediction and transition zone description were considered. If transition zone extension and flow characteristics within it can be described quite satisfied (especially accurate results can be obtained with correlation (12)), then correlation formulas for transition onset prediction lead to very big scatter and *a priori* predictions of transition coordinate with such correlations can provide too big (or even totally inadmissible) errors. Most of these criteria provide satisfactory results only for conditions close to the cases for which they were obtained. The lowest scatter in transition start locations was obtained with correlations (1′) and (3). Especially, the latter has to be noted as it has fixed set of constants for different supersonic and hypersonic flows — cold, hot, for slender and blunt bodies.

A number of modifications was proposed for laminar–turbulent transition model [4] allowing its application for hypersonic flow modeling. In any case, this model has empirical nature and it is some sophisticated way of incorporation of engineering correlations into the modern codes for solution of RANS equations that is very advantageous for description of LTT phenomena with RANS codes.

Effect of local heating/cooling on LTT transition on sharp cone was theoretically analyzed using both algebraic correlations and RANS models. It was

obtained for all these methods that heat supply to the boundary layer leads to additional stabilization of the hypersonic boundary layer and cooling gives rise to earlier transition. Presented results require further analysis and comparison of theoretical and numerical predictions with experimental results obtained within the framework of FP7 TransHyBeriAN project. This work was made as a part of this project with financial and management support of EU.

REFERENCES

1. Reshotko E. 2007. Transition issues for atmospheric entry. AIAA Paper No. 2007-0304.
2. Reshotko, E. 2009. Control of transition — I: Heating and cooling. VKI lectures on advances in laminar–turbulent transition modeling ser. RTO-EN-AVT-151-14. 1–18.
3. http://www.transhyberian.eu (accessed June 30, 2014).
4. Langtry, R., and F. Menter. 2009. Correlation-based transition modeling for unstructured parallelized computational fluid dynamics codes. *AIAA J.* 47(12):2894–2906.
5. Menter, F. R. 1994. Two-equation eddy-viscosity turbulence models for engineering applications. *AIAA J.* 32(8):1598–1605.
6. Schneider, S. P. 2004. Hypersonic laminar–turbulent transition on circular cones and scramjet forebodies. *Prog. Aerosp. Sci.* 40(1-2). 50 p. doi: 10.1016/j.paerosci.2003.11.001.
7. Thyson, N. A., and K. K. Chen. 1971. Extension of the Emmon's spot theory to flows on blunt bodies. *AIAA J.* 9(5):821–825.
8. Hirshel, E. H. 2005. *Basics of aerothermodynamics*. Berlin–Heidelberg: Springer Verlag. 426 p.
9. Hall, D. W., T. B. Harris, A. L. Murray, C. J. Wolf. 1982. Maneuvering Aerothermal Technology (MAT) program: A method for coupled three-dimensional inviscid and integral boundary layer calculations. BMO TR-82-37.
10. Goodrich, W. D., S. M. Derry, and J. J. Bertin. 1983. Shuttle orbiter boundary-layer transition: A comparison of flight and wind-tunnel data. AIAA Paper No. 83-0485.
11. Reshotko, E. 2007. Is $\mathrm{Re}_\theta/\mathrm{M}_e$ a meaningful transition criterion? AIAA Paper No. 2007-943. 9 p.
12. Kozlovsky, V. A., B. A. Zemlyansky, V. V. Kudryavtsev, and V. N. Shmanenkov. 2011. Investigation of boundary layer transition in three-dimensional supersonic flow over sharp cone. *7th European Symposium on Aerothermodynamics Proceedings*. Brugge, Belgium. ESA CP-692.
13. Lipnitskii, Yu. M., A. V. Krasilnikov, A. N. Pokrovskii, and V. N. Shmanenkov. 2003. *Unsteady aerodynamics of ballistic flight*. Moscow: Fizmatlit. [In Russian.]
14. Beckwith, I. E., and M. H. Bertram. 1972. A survey of NASA Langley studies on high-speed transition and the quiet tunnel. NASA TM X-2566. 67 p.

15. Johnson, H. B., G. V. Candler, and M. L. Hudson. 1997. Numerical study of hypersonic boundary layer transition on a blunt body. AIAA Paper No. 97-0554. 18 p.
16. Reda, D. C. 1981. Correlation of nosetip boundary-layer transition data measured in ballistics-range experiments. *AIAA J.* 19(3):329–339.
17. Reda, D. C., M. C. Wilder, D. W. Bogdanoff, and D. K. Prabhu. 2008. Transition experiments on blunt bodies with distributed roughness in hypersonic free flight. *J. Spacecraft Rockets* 45(2):210–215. doi: 10.2514/1.30288.
18. Singer, B. A. 1993. Modeling the transition region. NASA CR 4492.
19. Safiullin, R. A. 1971. Heat transfer in the region of laminar–turbulent transition. *Izv. USSR Acad. Sci. MZhG* 6:92–96. [In Russian.]
20. Dey, J., and R. Narasimha. 1990. An integral method for the calculation of two-dimensional transitional boundary layers. *J. Aircraft* 27(10):859–865. doi: 10.2514/3.45949.
21. Narasimha, R., and J. Dey. 1989. Transition zone models for 2-dimensional boundary layers: A review. *Sadhana* 14(2):93–120.
22. Cebeci, T. 2004. Analysis of turbulent flows. Berlin–Heidelberg: Elsevier. 384 p.
23. Arnal, D. 1988. Laminar–turbulent transition problems in supersonic and hypersonic flows. AGARD-FDP-VKI special course on aerothermodynamics of hypersonic vehicles.
24. Abu-Ghannam, B. J., and R. Shaw. 1980. Natural transition of boundary layers — the effects of turbulence, pressure gradient, and flow history. *J. Mech. Eng. Sci.* 22(5):213–228.
25. Mayle, R. E. 1991. The role of laminar–turbulent transition in gas turbine engines. *J. Turbomach.* 113:509–537.
26. Van Driest, E. R., and C. B. Blumer. 1963. Boundary layer transition — freestream turbulence and pressure gradient effects. *AIAA J.* 1(6):1303–1306. doi: 10.2514/3.1784.
27. Zhang, X., Z. Gao, and B. Zhong. 2012. Extensions of Menter's SST transition model to simulate hypersonic and crossflow transition. *ICAS 2012.* Brisbane, Australia.
28. Fisher, M. C. 1970. An experimental investigation of boundary-layer transition on a 10° half-angle cone at Mach 6.9. NASA TN D-5766.
29. Johnson, H. B., C. R. Alba, G. V. Candler, M. MacLean, T. Wadhams, and M. Holden. 2008. Boundary-layer stability analysis of the hypersonic international flight research transition experiments. *J. Spacecraft Rockets* 45(2):228–236. doi: 10.2514/1.31878.
30. Horvath, T. J., S. A. Berry, B. R. Hollis, Ch.-L. Chang, and B. A. Singer. 2002. Boundary layer transition on slender cones in conventional and low disturbance Mach 6 wind tunnels. AIAA Paper No. 2002-2743. 23 p.
31. Kimmel, R. L. 1993. The effect of pressure gradients on transition zone length in hypersonic boundary layer. WL-TR-94-3012. 35 p.
32. Stainback, P., M. Fisher, and R. Wagner. 1972. Effects of wind-tunnel disturbances on hypersonic boundary transition. AIAA Paper No. 72-181.

33. Borovoy, V. Ya., Yu. Yu. Kolochinskiy, and L. V. Yakovleva. 1982. Studying of unit Reynolds number effect on boundary layer transition on sharp cone. *Izv. USSR Acad. Sci. MZhG* 4. [In Russian.]
34. DeCarlo, J. P., R. J. Sanator, and D. T. Torrillo. 1965. Hypersonic boundary-layer transition data for a cold-wall slender cone. *AIAA J.* 3(4):758–760.
35. Stetson, K. F., and G. H. Rushton. 1967. Shock tunnel investigation of boundary-layer transition at M = 5.5. *AIAA J.* 5(5):899–906.
36. Softly, E. J., B. C. Graber, and R. E. Zempel. 1968. Experimental observation of transition of the hypersonic boundary layer. AIAA Paper No. 68-39.
37. Reda, D. C. 1978. Boundary-layer transition experiments on sharp, slender cones in supersonic freeflight. AIAA Paper No. 78-1129. 8 p.
38. Potter, J. L. 1968. Observations on the influence of ambient pressure on boundary-layer transition. *AIAA J.* 6(10):1907–1911.
39. Sheetz, Jr., N. W. 1969. Ballistics range boundary-layer transition measurements on cones at hypersonic speeds. *Symposium on Viscous Drag Reduction Proceedings.* Ed. C. S. Wells. Plenum Press. 53–83.
40. Johnson, C. B., P. C. Stainback, K. C. Wicker, and L. R. Boney. 1972. Boundary-layer edge conditions and transition Reynolds number data for a flight test at Mach 20 (reentry F). NASA TM X-2584. 84 p.